

# Localized incorporation of outer membrane components in the pathogen *Brucella abortus*

Victoria Vassen<sup>1</sup>, Claire Valotteau<sup>2</sup>, Cécile Feuillie<sup>2</sup>, Cécile Formosa-Dague<sup>2</sup>, Yves F Dufrêne<sup>2,3</sup> & Xavier De Bolle<sup>1,\*</sup> 

## Abstract

The zoonotic pathogen *Brucella abortus* is part of the Rhizobiales, which are alpha-proteobacteria displaying unipolar growth. Here, we show that this bacterium exhibits heterogeneity in its outer membrane composition, with clusters of rough lipopolysaccharide co-localizing with the essential outer membrane porin Omp2b, which is proposed to allow facilitated diffusion of solutes through the porin. We also show that the major outer membrane protein Omp25 and peptidoglycan are incorporated at the new pole and the division site, the expected growth sites. Interestingly, lipopolysaccharide is also inserted at the same growth sites. The absence of long-range diffusion of main components of the outer membrane could explain the apparent immobility of the Omp2b clusters, as well as unipolar and mid-cell localizations of newly incorporated outer membrane proteins and lipopolysaccharide. Unipolar growth and limited mobility of surface structures also suggest that new surface variants could arise in a few generations without the need of diluting pre-existing surface antigens.

**Keywords** *Brucella*; lipopolysaccharide; outer membrane; unipolar growth

**Subject Categories** Membrane & Intracellular Transport; Microbiology, Virology & Host Pathogen Interaction

DOI 10.15252/embj.2018100323 | Received 23 July 2018 | Revised 29 November

2018 | Accepted 4 December 2018

The EMBO Journal (2019) e100323

## Introduction

Cellular envelope growth is an essential feature of all organisms in order to increase in size and to divide afterward in order to generate daughter cells. Bacteria display different modes of growth. The model organism *Escherichia coli* incorporates new material dispersed along the sidewalls of the cell during elongation, typical for lateral growth (Burman *et al*, 1983; Woldringh *et al*, 1987; Wientjes & Nanninga, 1989; de Pedro *et al*, 1997). The old poles are thus composed of old envelope material, whereas the rest of the cell is a mixture of old and new inserted material. In contrast, bacteria

belonging to the order Rhizobiales are characterized by unipolar growth (Brown *et al*, 2012), in which the insertion of new outer membrane (OM) material during elongation takes place at one pole, namely the new pole. This leads to an asymmetric distribution of cell wall material after division, where one daughter cell is comprised mostly, if not exclusively, of new material and the pre-existing cell, the mother cell, retains the old envelope components.

*Brucella abortus* is an  $\alpha$ -proteobacterium and one of the etiological agents of brucellosis, a worldwide spread zoonosis infecting domestic and wildlife cattles (Moreno & Moriyón, 2006). Together with the other tested Rhizobiales, e.g., *Agrobacterium tumefaciens*, *Sinorhizobium meliloti* and *Ochrobactrum anthropi*, labeling with Texas Red-X succinimidyl ester (TRSE) revealed the new pole and the constriction site as proposed growth sites during elongation and division, respectively (Brown *et al*, 2012). TRSE is covalently binding to reactive amines accessible on the bacterial surface.

The OM of Gram-negative bacteria is an asymmetric bilayer with phospholipids on the inner leaflet and lipopolysaccharide (LPS) on the outer leaflet (Beveridge, 1999). This structure acts classically as a permeability barrier (Nikaido & Vaara, 1985) and is among other things involved in the interactions between pathogens and their hosts. LPS is composed of lipid A, linked to the core, to which the O-chain, also called O-polysaccharide, is attached. The LPS of *Brucella* differs from the classical LPS of *E. coli* (as reviewed in Lapaque *et al*, 2005). For instance, the lipid A of *Brucella* LPS contains longer acyl chains (Lapaque *et al*, 2005) and the core is a branched structure (Conde-Alvarez *et al*, 2012). Moreover, the LPS of *Brucella* has only a low endotoxic activity (see review; Lapaque *et al*, 2005; Cardoso *et al*, 2006) compared to *E. coli* LPS.

In general, the most variable part of LPS is the O-chain, which in *Brucella* is an unbranched homopolymer of *N*-formyl-perosamine (Moreno & Moriyón, 2006). If the O-chain is attached to the LPS core, it is classified as smooth LPS (S-LPS). The more relevant zoonotic species, *B. abortus*, *Brucella melitensis* and *Brucella suis*, have a smooth phenotype (Moreno & Moriyón, 2006). Based on investigations of LPS extractions of several smooth *Brucella* strains on SDS-PAGE, the length of the O-chain can highly vary inside a single population and between species (Dubray & Limet, 1987; Bowden *et al*, 1995). In contrast, if the O-chain is missing and LPS is only made of

<sup>1</sup> Research Unit in Biology of Microorganisms (URBM), Narilis, University of Namur (UNamur), Namur, Belgium

<sup>2</sup> Louvain Institute of Biomolecular Science and Technology, Université catholique de Louvain (UCL), Louvain-la-Neuve, Belgium

<sup>3</sup> Walloon Excellence in Life Sciences and Biotechnology (WELBIO), Wavre, Belgium

\*Corresponding author. Tel: +32 81 44 38; E-mail: xavier.debolle@unamur.be

lipid A and core, it is named rough LPS (R-LPS). The naturally occurring rough species identified so far, *Brucella ovis* and *Brucella canis*, have a reduced virulence to their specific hosts (Moreno & Moriyón, 2006). Dissociation from S-LPS to R-LPS was reported to occur in culture and during infection in *Brucella* (Turse *et al*, 2011).

Besides LPS, the OM is also composed of outer membrane proteins (Omps). It was estimated that they cover around 25% of the bacterial surface in *E. coli* (Amro *et al*, 2000). Recently, it was shown that Omps of *E. coli* is organized in Omps clusters, which are homogeneously distributed over the cell (Rassam *et al*, 2015). These Omps clusters are only moving due to the insertion of new Omp islands pushing pre-existing islands to the cell poles, highlighting the low mobility of Omps in the OM (Rassam *et al*, 2015). In *B. abortus*, there are two major Omps identified, Omp25 and Omp2b (Dubray & Bezard, 1980), which are both exposed at the cell surface. The function of the non-essential Omp25 is not identified yet, whereas the essential porin Omp2b forms trimers in the OM and is proposed to be involved in nutrient uptake (Douglas *et al*, 1984; Mobasher *et al*, 1997).

In the present study, the surface of the OM of *B. abortus* was analyzed using immunofluorescence (IF), flow cytometry, and atomic force microscopy (AFM) allowing the characterization of the topography of the cell surface at the nanoscale level. These analyses reveal heterogeneity in the OM, in which clusters of Omp2b co-localize with R-LPS. Moreover, insertion sites of Omp25, peptidoglycan (PG) and LPS are found to be located to the new pole and to the division site. Interestingly, Omp25 and Omp2b, and LPS do not diffuse from their primary insertion sites, showing the absence of long-range diffusion of these major components of the *B. abortus* OM. This characteristic has consequences for the generation of daughter cells with a different surface antigen.

## Results

### The OM of *Brucella abortus* is heterogeneous

In order to investigate the structure of the OM of the smooth *B. abortus* 544 wild-type (WT) strain (Moreno & Moriyón, 2006), the presence of S-LPS and R-LPS on the bacterial surface was investigated by IF and flow cytometry. The specificities of the monoclonal antibodies (mAbs) were checked (Appendix Fig S1) and were consistent with previous data (Cloeckaert *et al*, 1992a, 1993). The mAb specific for R-LPS recognizes the lateral branch of the core (Gil-Ramírez *et al*, 2014) in the absence of the O-chain; thus, the characteristic higher molecular weight bands of S-LPS are not detected in Western blot (Appendix Fig S1A). Co-localization of S-LPS and R-LPS by IF showed strikingly different localization patterns. S-LPS was homogeneously distributed, whereas R-LPS showed a heterogeneous distribution along the cell ( $n = 477$  bacteria) (Figs 1A and EV1). Localization of R-LPS can differ from full labeling to partial or patchy labeling. Nevertheless, both LPS types are co-localizing with S-LPS present in R-LPS clusters.

The high diversity in the proportion of R-LPS on the bacterial surface could also be detected by flow cytometry using bacteria labeled with mAbs specific for S-LPS and R-LPS (Fig 1B). Indeed, the fluorescence intensity corresponding to R-LPS presented a wider distribution in comparison to the S-LPS fluorescence (Coefficient

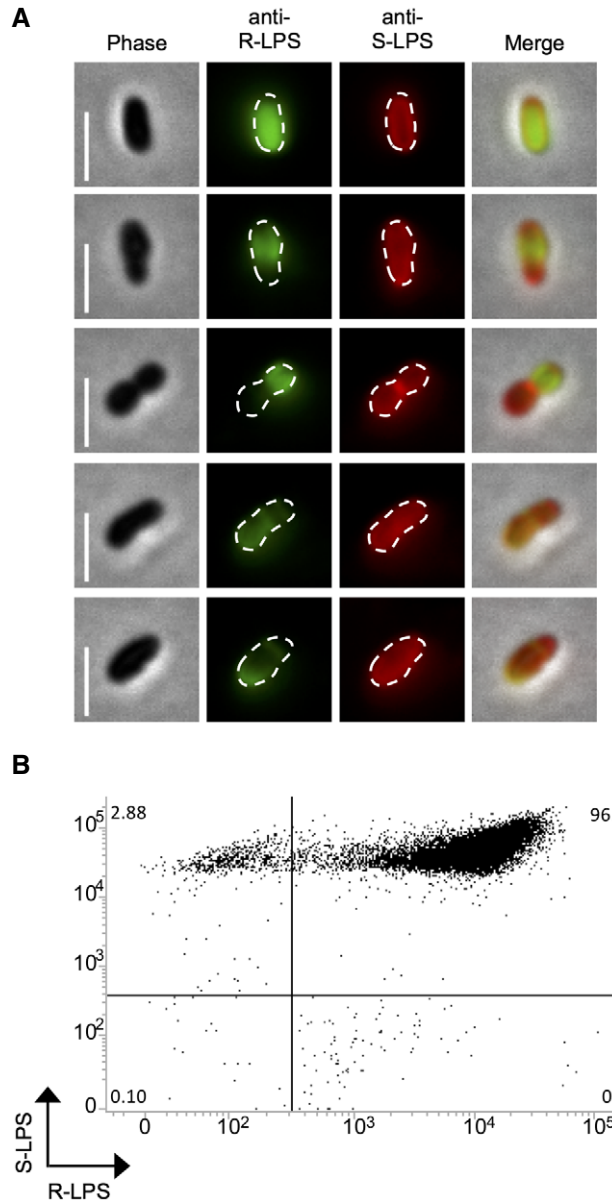


**Figure 1. Heterogeneity of the OM of the smooth *B. abortus* wild-type strain.**

- A Localization of R-LPS (green) and S-LPS (red) in exponential phase bacteria. Scale bars: 2  $\mu$ m.
- B Distribution of R-LPS and S-LPS in exponential phase culture analyzed by flow cytometry (one representative example among three biological replicates,  $n = 20,000$  events). Numbers in each corner correspond to % of relative frequencies.

of variation  $CV_{R-LPS} = 75.8 \pm 13.8\%$  (mean  $\pm$  SD) and  $CV_{S-LPS} = 46.8 \pm 4.5\%$  (mean  $\pm$  SD),  $n = 3$  independent experiments, 20,000 events each). This was consistent with a higher variability in the R-LPS distribution among the bacterial cells. In general,  $97.4 \pm 1.1\%$  (mean  $\pm$  SD,  $n = 3$  independent experiments, 20,000 events each) of the population in an exponential growth phase could be classified as containing a mix of S-LPS and R-LPS under this condition. Only  $2.2 \pm 0.9\%$  (mean  $\pm$  SD) were exclusively smooth and  $0.2 \pm 0.3\%$  (mean  $\pm$  SD) were exclusively rough in exponential growth phase.

The presence of R-LPS molecules on the bacterial surface could also be associated with an increase in surface roughness, thus leading to an irregular surface due to the co-localization of R-LPS and S-LPS (Fig 2). This phenomenon can be measured by AFM coupled to fluorescence microscopy. Thanks to the ability of AFM to perform high-resolution imaging, it is possible using this technology to get access to quantifiable surface structure information such as roughness (Formosa *et al.*, 2012). The average roughness ( $R_a$ ) was measured on bacteria labeled with the mAb specifically recognizing R-LPS. Areas enriched in R-LPS in the WT strain (R-LPS<sup>+</sup> area), identified by fluorescence microscopy, displayed a more irregular surface and therefore a higher  $R_a$  (Figs 2A and B, and EV2A). This is consistent with a high abundance of short R-LPS (without O-chain) mixed with long S-LPS (with O-chain) in the same area. Their roughness ( $R_a = 7.4 \pm 3.2$  nm (mean  $\pm$  SD),  $n = 13$  bacteria) appears systematically higher than for the unlabeled areas (R-LPS<sup>-</sup> area,  $R_a = 4.5 \pm 1.6$  nm (mean  $\pm$  SD),  $n = 13$  bacteria), without detectable R-LPS by IF (Fig 2A and B). A higher amount of R-LPS molecules in the WT increased the  $R_a$  by about 1.6-fold. As a positive control, the rough mutant strain *B. abortus*  $\Delta gmd$ , lacking the GDP-mannose dehydratase Gmd involved in the LPS O-chain biosynthesis (Godfroid *et al.*, 2000) and thus having only R-LPS, was used (Appendix Figs S1 and S2). Similar to the WT cells, two areas were analyzed per bacterium (Fig 2A and B) and both, area 1 and area 2, showed a low roughness [Fig 2B,  $R_a$  area 1 =  $2.8 \pm 0.8$  nm (mean  $\pm$  SD),  $R_a$  area 2 =  $3.4 \pm 1$  nm (mean  $\pm$  SD),  $n = 7$  bacteria]. These low  $R_a$  values are consistent with a homogeneous R-LPS layer on the mutant strain (Ratio of roughness close to 1, Fig EV2A). Moreover, unlabeled WT and  $\Delta gmd$  cells were analyzed revealing similar differences of roughness between the two areas in the WT and minor differences in unlabeled  $\Delta gmd$  cells (Fig EV2B–D). This indicates that labeling with the mAb does not strongly affect the measured  $R_a$  values.

In addition, multiparametric imaging that offers the possibility to image the surface structure while mapping their adhesive properties at high-spatial resolution (Chopinet *et al.*, 2013), was performed on unlabeled WT cells with AFM tips functionalized with the anti-R-LPS mAb (see Materials and Methods for details). Using this advanced AFM mode, it is then possible to directly link adhesive events with the presence of R-LPS on the cell surface and quantify them as the percentage of adhesion,  $P_{adh}$  (Fig 2C and D). On each cell, the areas with the lower  $R_a$  indicating a more regular surface structure were assigned area 1 ( $R_a$  area1 =  $1.4 \pm 0.5$  nm (mean  $\pm$  SD),  $n = 9$  bacteria), whereas the areas with the higher  $R_a$  and thus a more irregular surface were determined as area 2 ( $R_a$  area2 =  $4.7 \pm 3.1$  nm (mean  $\pm$  SD),  $n = 9$  bacteria), respectively. We observed that this distinction was correlated with a statistically significant difference in  $P_{adh}$ , with the irregular surface area (area 2) showing a higher  $P_{adh}$  than the uniform area (area 1) ( $P < 0.05$ ). This result is consistent with an increased roughness in presence of R-LPS clusters in the heterogeneous surface structure.

### Clusters of R-LPS are co-localizing with the essential Omp2b

Given the heterogeneous localization of R-LPS on the *B. abortus* cell surface (Fig 1A), we were interested in investigating the localization of other OM components. Interestingly, one of the major Omp, the essential porin Omp2b (Douglas *et al.*, 1984), also displayed a

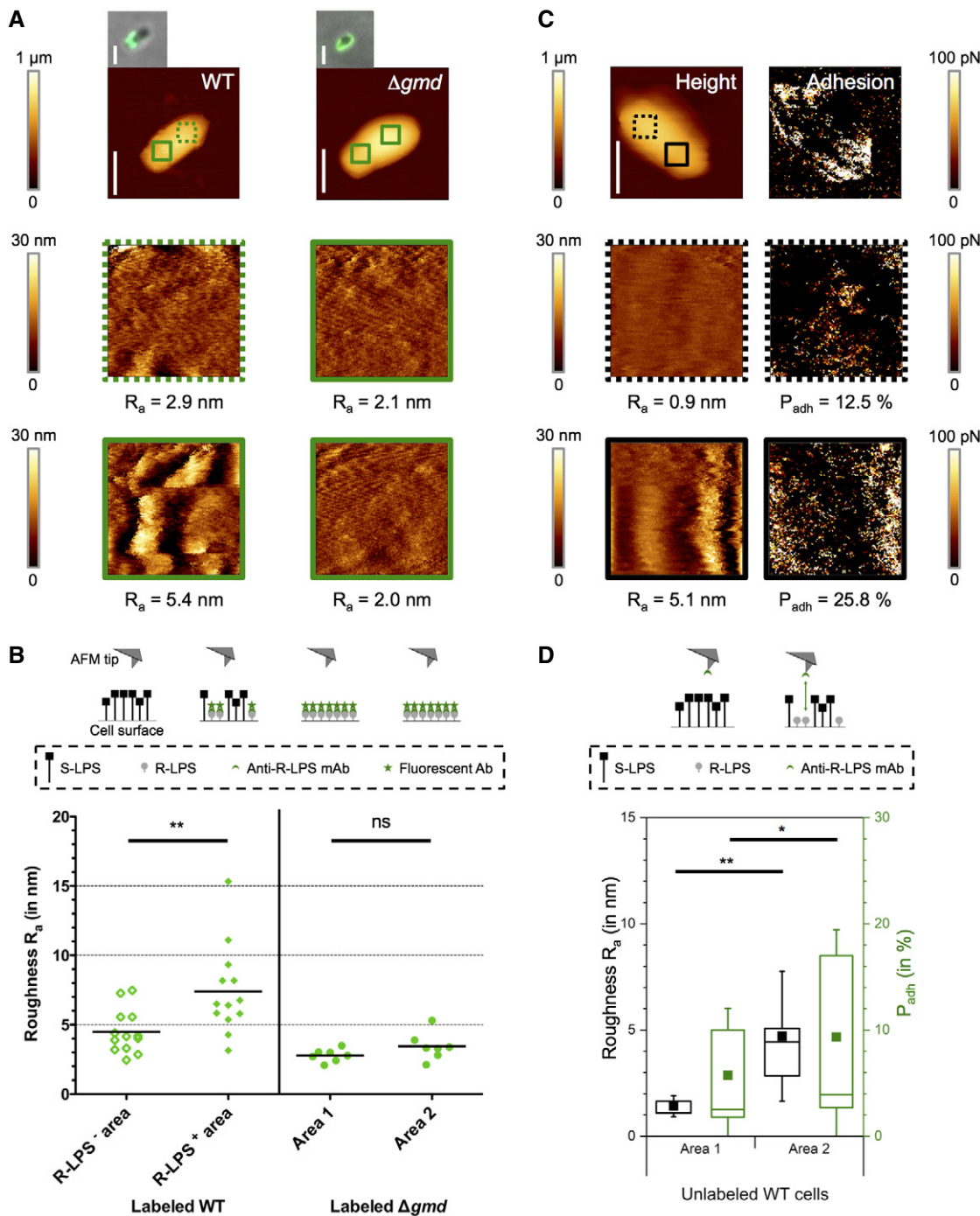
heterogeneous distribution when localized with mAb (A68/15B06/C08) directed against Omp2b (Paquet *et al.*, 2001) by IF (Fig 3A). Similar to the R-LPS distribution, there was also a high diversity of distributions ranging from full to partial or patchy localization. This was also found in the rough strain  $\Delta gmd$ , suggesting that the patchy labeling is not an artifact due to the steric hindrance of mAb binding to Omp2b by S-LPS. Labeling with another mAb (A68/25G05/A05) also directed against Omp2b (Cloeckaert *et al.*, 1990) showed the same heterogeneity in localization. We thus wondered whether Omp2b and R-LPS could be co-localized. We observed that it was indeed the case, as they displayed co-localization patterns in double labeling IF experiments (Fig 3A). When analyzing the Pearson correlation coefficient (PCC)  $r$  between Omp2b and R-LPS fluorescence signals, 71.9% (318/442 bacteria) of an exponential phase culture showed a PCC  $r$  significantly higher than 0 ( $P < 0.01$ ) and therefore a positive linear correlation. Analysis of the fluorescence intensities at each pixel indicated that the number of pixels that are positive for the two labelings is threefold more abundant than expect by chance (i.e., under the null hypothesis of independent labelings), which is statistically significant ( $\chi^2 = 10,729$ ,  $P < 10^{-10}$ , 1 degree of freedom).

The co-localization of R-LPS and Omp2b was also investigated by AFM. Omp2b was detected by IF in order to determine Omp2b positive (Omp2b<sup>+</sup>) and negative (Omp2b<sup>-</sup>) areas on individual cells. The AFM tip was functionalized with the mAb directed against R-LPS (Cloeckaert *et al.*, 1993) and the interaction between the tip and the cell surface was measured (Fig 3B). On the WT cells, the  $P_{adh}$  value, correlating to the detection of R-LPS, was higher in Omp2b<sup>+</sup> areas ( $P_{adh} = 15.4 \pm 7.0\%$  (mean  $\pm$  SD),  $n = 13$  bacteria) compared to Omp2b<sup>-</sup> areas ( $P_{adh} = 8.7 \pm 5.3\%$  (mean  $\pm$  SD),  $n = 13$  bacteria) (Appendix Fig S3 for a comprehensive summary), with a ratio Omp2b<sup>+</sup>/Omp2b<sup>-</sup> of  $3.0 \pm 3.8$  (mean  $\pm$  SD,  $n = 13$  bacteria, Fig 3C). This is consistent with the enrichment of R-LPS in the Omp2b<sup>+</sup> areas. As a positive control, the mutant strain  $\Delta gmd$  expressing only R-LPS was imaged with the same tip. A  $P_{adh}$  ratio Omp2b<sup>+</sup>/Omp2b<sup>-</sup> close to 1 ( $1.1 \pm 0.7$  (mean  $\pm$  SD),  $n = 13$  bacteria) was obtained (Fig 3C), as expected for a homogeneous cell surface composed of only R-LPS. This result further corroborates a co-localization of Omp2b and R-LPS clusters on WT cells.

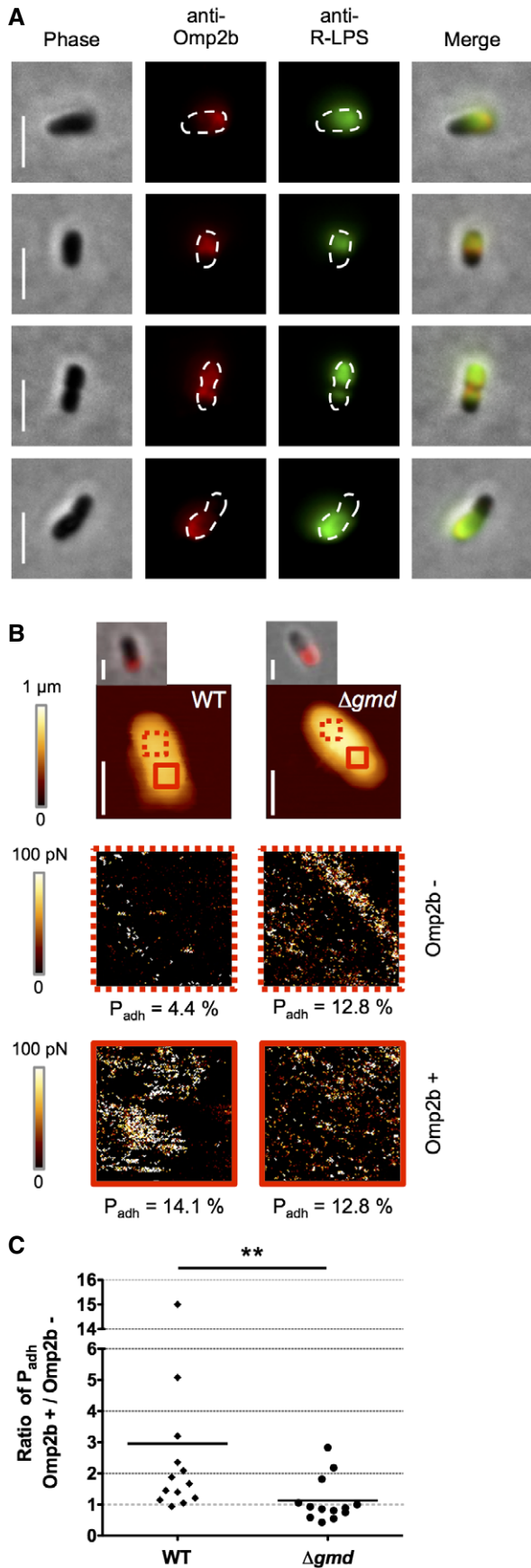
### Unipolar insertion of Omp25 and absence of long-range diffusion of Omps

It is known that in the order Rhizobiales, labeling of bacteria with TRSE and follow up of subsequent growth in the absence of the dye indicates that new OM components are incorporated at the new pole and at the constriction site (Brown *et al.*, 2012). However, the nature of the OM compounds labeled with TRSE is unknown, and the incorporation of specific components has never been investigated to our knowledge.

During the analysis of the localization of OM components by IF, Omp25, one of the major Omp of *B. abortus* (Dubray & Bezard, 1980), was found to have a homogenous distribution [ $83.7 \pm 8.2\%$  (mean  $\pm$  SD),  $n = 479$  bacteria, five biological replicates] on the cell surface (Fig 4A, panel 0 h), suggesting that it is continuously produced during the cell cycle like previously reported (Francis *et al.*, 2017). The specificity of the anti-Omp25 mAb (Cloeckaert *et al.*, 1990) was additionally confirmed by IF and Western blot with

**Figure 2. Differences in surface structure of the OM investigated by AFM.**

- A Roughness measurements on R-LPS labeled (green) WT and  $\Delta gmd$  cells. AFM images of whole bacteria and of the separated areas (colored squares in first images,  $0.4 \times 0.4 \mu\text{m}^2$ ) are shown. The arithmetic roughness  $R_a$  is indicated below each area. Scale bars: 1  $\mu\text{m}$ .
- B Quantitative roughness measurement of R-LPS labeled WT and  $\Delta gmd$  cells. The areas with the lower roughness (more regular surfaces) of  $\Delta gmd$  cells were assigned as areas 1. mAb: monoclonal antibody. Ab: antibody.  $n_{WT} = 13$  bacteria.  $n_{\Delta gmd} = 7$  bacteria. Differences were statistically analyzed by t-test. \*\* $P < 0.01$ . ns: not significant.
- C Detection of forces between AFM tip functionalized with mAb against R-LPS and unlabeled WT cells. Height image and the corresponding adhesion image are shown on top and zooms of depicted areas (black squares,  $0.4 \times 0.4 \mu\text{m}^2$ ) below. The arithmetic roughness  $R_a$  and percentage of adhesion  $P_{adh}$  are indicated below each area. Scale bar: 1  $\mu\text{m}$ .
- D Correlation between roughness and detection of R-LPS on unlabeled WT cells. The areas with the lower roughness (more regular surfaces) were assigned as areas 1. The boxplot represents the mean values (squares), the median (horizontal line), the 25 and 75% quartiles (box limits) and the standard deviations (whiskers).  $n = 9$  bacteria. Error bars: SD. Statistical differences were analyzed by t-test. \*\* $P < 0.01$ . \* $P < 0.05$ .

**Figure 3. Co-localization of R-LPS and the essential porin Omp2b.**

A Co-localization of Omp2b (red) and R-LPS (green) in exponential phase bacteria. Scale bars: 2  $\mu\text{m}$ .  
B Co-detection of Omp2b (red) and R-LPS by AFM. R-LPS was detected using AFM tips functionalized with mAb against R-LPS. AFM images of whole bacteria and of the separated areas (red squares in first images,  $0.4 \times 0.4 \mu\text{m}^2$ ) are shown. The percentages of adhesion  $P_{\text{adh}}$  are indicated below each area. Scale bars: 1  $\mu\text{m}$ .  
C Adhesion ratio between the Omp2b positive area compared to the Omp2b negative area. Gray dashed line shows ratio = 1 corresponding to homogeneity in surface structure.  $n_{\text{WT}} = 13$  bacteria,  $n_{\Delta gmd} = 13$  bacteria. Statistical analysis with Mann–Whitney U-test showed \*\* $P < 0.01$ .

the deletion strain *B. abortus*  $\Delta$ omp25 (Appendix Fig S4). The mAb directed against Omp25 can therefore be used to monitor the incorporation of Omp25 in the OM by labeling the pool of pre-existing Omp25 followed by a period of growth incorporating new Omp25, which are unlabeled (the antibody was removed before growth was resumed). TRSE-labeled bacteria were labeled by IF with the mAb directed against Omp25. Initially, Omp25 was homogeneously distributed on the bacterial surface (Fig 4A, panel 0 h). Bacteria labeled with TRSE and anti-Omp25 mAb were further grown in the absence of both labelings, generating an envelope that is not labeled with Texas Red at the new pole for most of the cells, at the constriction site and new pole or rarely at the constriction site only (Fig 4A and B). Interestingly, these TRSE-negative regions mapped with areas negative for the Omp25 labeling [PCC  $r = 0.88 \pm 0.03$  (mean  $\pm$  SD),  $n = 279$  bacteria]. Newly incorporated, and therefore unlabeled, Omp25 was mostly incorporated at the new pole [ $79.8 \pm 6.5\%$  (mean  $\pm$  SD),  $n = 279$  bacteria] and/or at the constriction site under these experimental conditions (Fig 4C). The labeling with TRSE had no severe impact on incorporation of new Omp25 (Fig 4A, second panel 2 h) suggesting that TRSE-negative areas indeed comprise newly incorporated, unlabeled Omp25. In this experiment, the proportion of bacteria displaying a homogeneous distribution of Omp25 was  $67.1 \pm 7.9\%$  (mean  $\pm$  SD,  $n = 660$  bacteria, three biological replicates) and was slightly decreased in comparison with the previous experiment (Fig 4A, panel 0 h). This could be explained by a later phase in culture (2 h of additional growth in Fig 4A, second panel 2 h). The co-existence of Omp25-positive and Omp25-negative areas on the same bacterium showed that this protein does not exhibit long-range diffusion on the bacterial surface. Moreover, the heterogeneously distributed Omp2b was also not moving into the TRSE-negative areas in IF experiments (Figs 4D and EV3). This could be statistically confirmed by analyzing the distribution of Omp25- and Omp2b-positive pixels in areas positive and negative for TRSE, showing that Omp25 and Omp2b do not co-localize with TRSE-negative zones (Fig 4E,  $P < 0.001$ ).

Taken together, these results allow us to propose that at least two major Omps of *B. abortus* are poorly mobile on the bacterial surface in time and space scales applied in these experiments.

#### PG is inserted at the same sites than Omp25

Furthermore, the incorporation of new PG was investigated using the fluorescent D-amino acid HCC-amino-D-alanine (HADA), allowing an efficient labeling of newly synthesized PG (Kuru

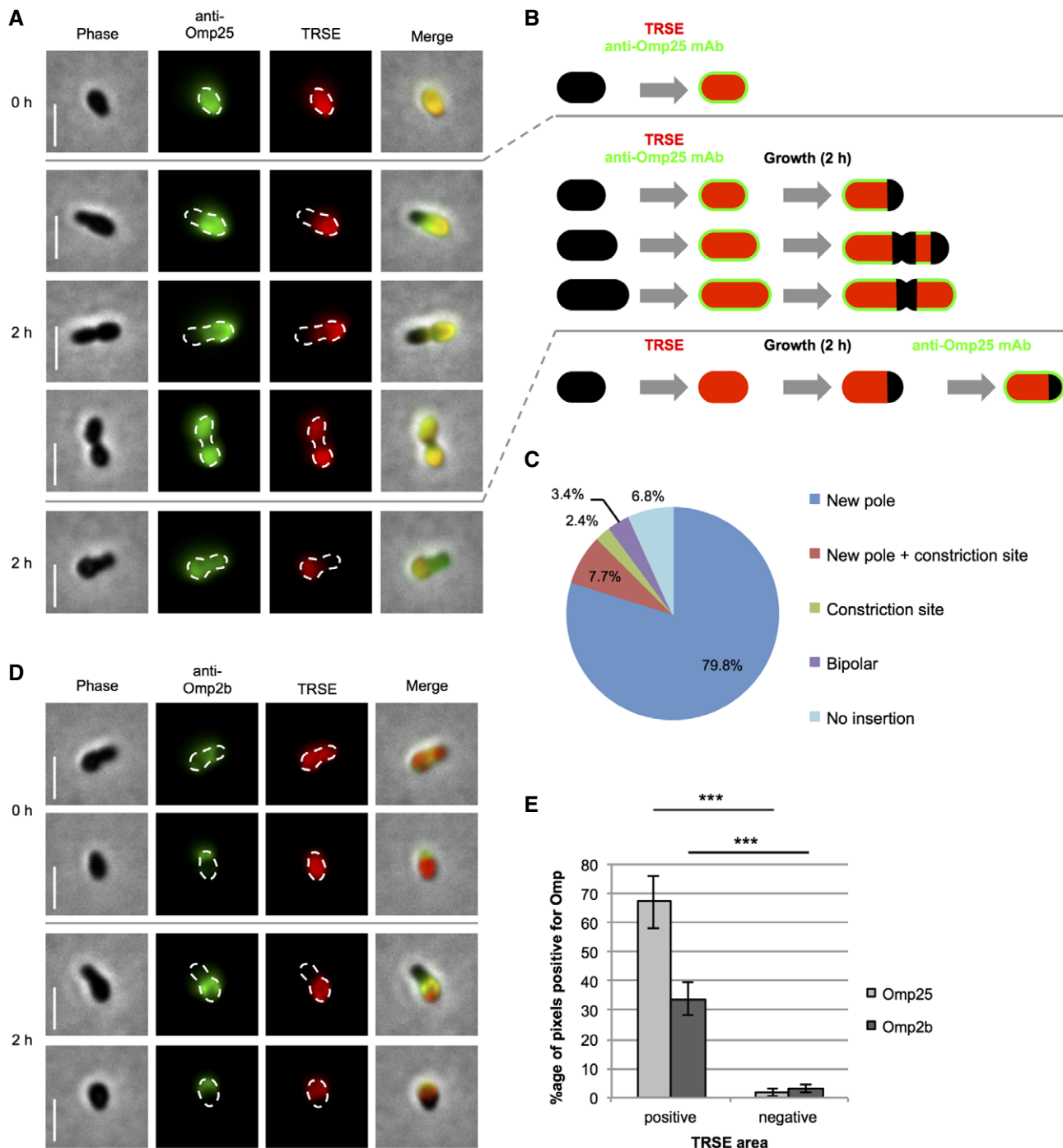


**Figure 4.** Unipolar insertion of Omp25 and low mobility of Omp25 and Omp2b.

- A Localization of initially labeled Omp25 (green) on TRSE-labeled (red) bacteria before (0 h) and after 2 h of growth in the absence of both labelings (2 h). As a control, Omp25 localization after pulse-chase labeling with TRSE is shown at the bottom panel. Scale bars: 2  $\mu$ m.
- B Model of TRSE (red) and Omp25 (green) labeling corresponding to (A). Incorporation of new material at the pole and/or at the constriction site is shown as black areas.
- C Quantification of localization of newly inserted Omp25 represented by negative Omp25 areas from (A). Numbers are indicating mean percentages.  $n = 279$  bacteria (five biological replicates).
- D Localization of initially labeled Omp2b (green) on TRSE-labeled (red) bacteria before (0 h) and after 2 h of growth in the absence of both labelings (2 h). Scale bars: 2  $\mu$ m.
- E Co-localization of Omp25- and Omp2b-positive pixels with TRSE-positive or TRSE-negative pixels, respectively. Error bars correspond to SD from independent experiments. Differences were statistically analyzed by t-test. \*\*\* $P < 0.001$ .  $n_{\text{Omp25}} = 279$  bacteria, 85,666 pixels (five biological replicates).  $n_{\text{Omp2b}} = 252$  bacteria, 74,630 pixels (three biological replicates).

*et al.*, 2012). Bacteria expressing the old pole marker PdhS-mCherry (Hallez *et al.*, 2007) were labeled for 5 min with HADA, fixed and analyzed by fluorescence microscopy. In agreement with the previously proposed growth sites, newly incorporated PG was inserted at the new pole and at the constriction site (Fig 5A and B). Analysis of the HADA fluorescence intensity showed a polar incorporation for most cells (Fig 5C). In longer cells, the PG insertion was directed to the mid-cell at the constriction site.

#### LPS is inserted at the growth sites and is not highly mobile

Since Omp25 and PG are inserted at the new pole and at the constriction site (Figs 4A and 5A), we wondered whether LPS was incorporated at the same growth areas. To answer this question, we constructed a  $\Delta gmd$  rough strain where the synthesis of S-LPS can be induced by controlling *gmd*. As indicated above, the absence of the O-chain and the rough phenotype of  $\Delta gmd$  were checked by IF using the mAb directed against S-LPS (Appendix Fig S1B) and by Western blot (Appendix Figs S1A and S2A). A copy of *gmd* was provided on a plasmid under the control of the *E. coli lac* promoter ( $p_{lac}\text{-}gmd$ ) and was therefore inducible with isopropyl  $\beta$ -D-1-thio-galactopyranoside (IPTG). Under normal growth conditions in rich medium, the  $\Delta gmd\ p_{lac}\text{-}gmd$  strain had a rough phenotype without detectable O-chain on its surface in the absence of IPTG (Fig 6A) and displayed a slight growth defect similar to the  $\Delta gmd$  parental strain (Appendix Fig S5A). As an indicator of growth, bacteria were labeled with eFluor dye, which is labeling the surface in a similar way as TRSE by covalent binding to accessible amines. When the strain was induced with IPTG for 4 h, a portion of bacteria displayed detectable S-LPS on their surface (Fig 6A). Empty vector negative controls are shown in Appendix Fig S5B. S-LPS localization by IF revealed that it was mostly detected at the new pole ( $66.9 \pm 1.8\%$  (mean  $\pm$  SD),  $n = 468$  bacteria), i.e., opposite to the

old pole marker PdhS-mCherry and in the eFluor negative part of the OM (Fig 6B and C). The S-LPS could also be detected at the constriction site (Fig 6A–C). A small proportion of bacteria showed S-LPS insertion at both poles ( $5.0 \pm 2.1\%$  (mean  $\pm$  SD),  $n = 468$  bacteria). This could be explained by the fact that if a divisional bacterium inserted new S-LPS at the new pole and the constriction site (see Fig 6A, Image 2  $\Delta gmd\ p_{lac}\text{-}gmd +$ IPTG) and directly divided afterward, one of the daughter cells would show a bipolar S-LPS labeling. Additionally, a minor population of the cells showed a homogenous S-LPS localization [ $2.1 \pm 1.7\%$  (mean  $\pm$  SD),  $n = 468$  bacteria] and only one bacterium [ $0.1 \pm 0.3\%$  (mean  $\pm$  SD),  $n = 468$  bacteria] was found to inserted S-LPS at the old pole. Consistent with the experiments described above showing the unipolar insertion of Omps and PG at the new pole and at the constriction site, here we show that LPS is also incorporated at these two growth sites. Observations reported in Fig 6A also suggest that S-LPS is displaying a very poor mobility within the time of the presented experiment (4 h). Indeed, a high mobility of S-LPS would have given homogeneously distributed S-LPS (with O-chain) on the bacterial surface after IPTG induction in the  $\Delta gmd\ p_{lac}\text{-}gmd$  strain (Fig 6A), which is not the case.

In order to study the mobility of R-LPS and S-LPS on the bacterial surface without mAbs that could be suspected to cluster O-chains together, we used a technique allowing the labeling of 3-deoxy-D-manno-octulosonic acid (Kdo), a sugar in the core of LPS, through click chemistry (Dumont *et al.*, 2012; Fugier *et al.*, 2015). A Kdo derivative carrying a N<sub>3</sub> group at position C8 (Kdo-N<sub>3</sub>) was added to the culture medium, taken up by the bacteria and incorporated in the biosynthesis of the LPS core of both S- and R-LPS. The N<sub>3</sub> groups can react with a fluorescent cyclooctyne derivative, allowing the localization of newly incorporated Kdo-N<sub>3</sub> on the bacterial surface (Dumont *et al.*, 2012; Fugier *et al.*, 2015). Bacteria were labeled with eFluor, grown for 2 h in the presence of Kdo-N<sub>3</sub>, and then labeled by a strained alkyne (cyclooctyne) fused to a

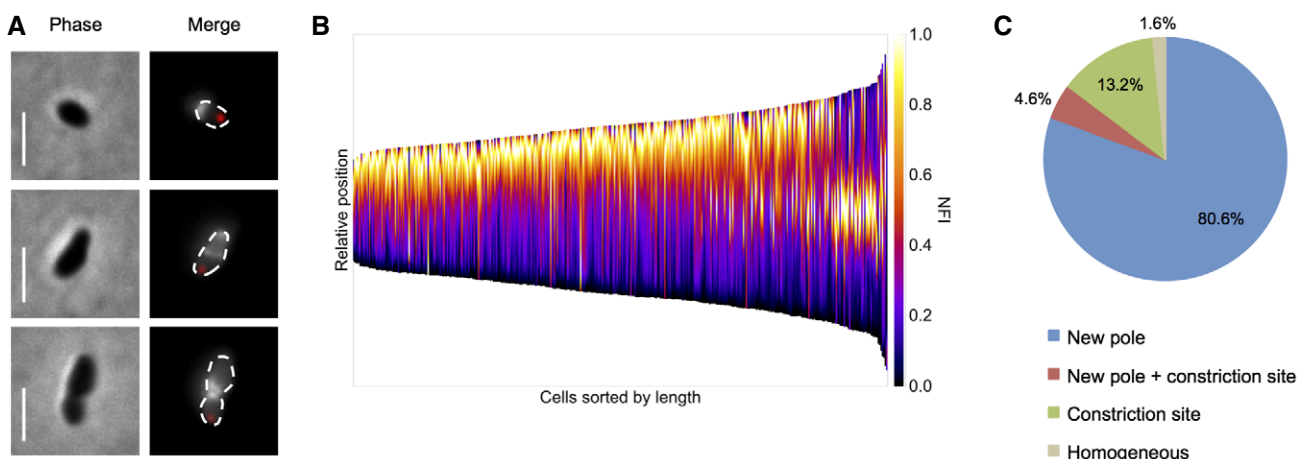


**Figure 5. Unipolar insertion of PG.**

- A Short pulse labeling of exponential phase bacteria with the fluorescent D-amino acid HADA. Merge is showing old pole marker PdhS-mCherry (red) and PG insertion sites (white). Scale bars: 2  $\mu$ m.
- B Demographic representation of HADA labeling. Bacteria were sorted according to their cell length and oriented with the old pole at the bottom of the demograph by PdhS-mCherry fluorescence signal. NFI: normalized fluorescence intensity.  $n = 393$  bacteria (three biological replicates).
- C Quantification of localization of PG insertion sites from (A). Numbers are mean percentages.  $n = 393$  bacteria (three biological replicates).

fluorophore (Fig 6D). The newly inserted LPS carrying Kdo-N<sub>3</sub> arose mostly from the new pole [75.1 ± 1.5% (mean ± SD), n = 566 bacteria], opposite to PdhS-mCherry and eFluor labeling, and occasionally from the constriction site (Fig 6E and F). Interestingly, there was heterogeneity within the population regarding the area covered by the Kdo-N<sub>3</sub> fluorescence, corresponding to a high proportion of the cell surface for some bacteria. This could be due to the variation in the amount of incorporated LPS among single bacteria (consistent with different growth rates for individual bacteria inside the population), or to a low diffusion rate or confinement diameter allowing newly incorporated LPS to cover more surface in a fraction of the bacteria in comparison with absent diffusion. The detection of a zonal labeling by Kdo-N<sub>3</sub> showed that LPS does not display long-range diffusion under the tested conditions.

A long pulse labeling with Kdo-N<sub>3</sub> confirmed this hypothesis. If bacteria were initially labeled with Kdo-N<sub>3</sub> and washed and growth was restarted in the absence of the dye, the newly inserted unlabeled LPS could be observed at the same growth sites, further supporting the main insertion of newly synthesized LPS at these sites (Fig EV4A and B). There were 17.7 ± 9.0% (mean ± SD, n = 924 bacteria), usually small in size that did not show an unlabeled area under these experimental conditions (Fig EV4B). This would be consistent with a low mobility of LPS in these cells. Nevertheless, the detection of unlabeled areas (Fig EV4A–C) showed the absence of LPS diffusion in a relative long period of time (2 h).

In conclusion, by the induction of S-LPS production in a rough strain as well as by the direct labeling of LPS, it could be shown that LPS is incorporated at the new pole and at the constriction site and that LPS seems to have a limited mobility.

Altogether, these data suggest that unipolar growth is not accompanied with a massive diffusion of the mother cell envelope into the daughter cell envelope. This low mobility of OM components could have important consequences for the generation of daughter cells with different surface components.

#### Efficient generation of daughter cells with a new surface component

Experiments described above show that the OM components such as Omp25, Omp2b, and LPS do not display long-range diffusion. This is consistent with the TRSE (or eFluor) labeling patterns, since initial TRSE labeling does not diffuse on the cell surface (Brown *et al*, 2012). One interesting consequence of this very low diffusion is that, in principle, producing daughter cells completely covered with a new antigen on their surface would require fewer generations compared to a classical diffusion (Fig EV5). If the surface components diffuse very slowly, it is predictable that if a switch in gene expression occurs in a mother cell with unipolar growth, this could generate daughter cells completely covered with a new surface component at the second generation (Fig EV5). To obtain a proof of principle of this assumption, the S-LPS inducible strain  $\Delta gmd$  *plac* $gmd$  was used to control the synthesis of the O-chain of S-LPS. Cultures were induced with IPTG and the presence of S-LPS and R-LPS on the bacterial surface was analyzed by flow cytometry and fluorescence microscopy by labeling with the mAbs directed against S-LPS and R-LPS (Cloeck-aert *et al*, 1993) (Fig 7). The non-induced control strain is shown in Appendix Fig S6. After 3 h of induction, bacteria analyzed by

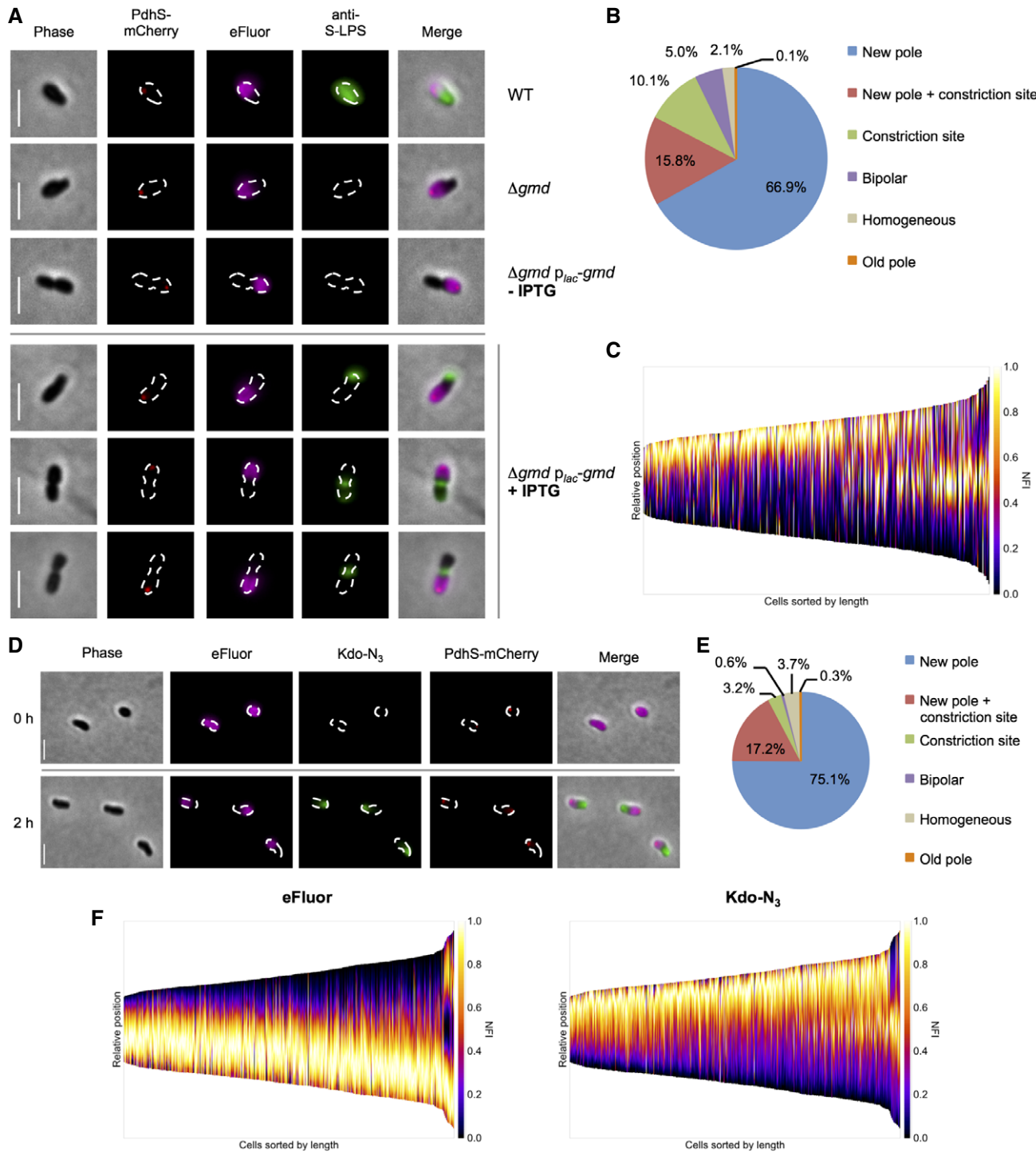
flow cytometry still showed a rough phenotype, probably because bacteria did not have the time to produce and translocate a detectable amount of S-LPS on the surface (Fig 7A). Then, after 6 h of induction, bacteria started to incorporate S-LPS on their surface, as shown by the increase of the proportion of bacteria with a positive S-LPS signal (Fig 7A). The majority of the population contained also S-LPS as early as 9 h. After 24 h, most bacteria possessed a mix of S-LPS and R-LPS on their surfaces similar to the WT (Fig 1B). At 9 h post-induction, the proportion of bacteria fully labeled with the S-LPS mAb was 39.4 ± 4.3% (mean ± SD, n = 937 bacteria) and reached 54.9 ± 4.4% (mean ± SD, n = 1059 bacteria) after 24 h post-induction (Fig 7B). It is thus remarkable that a 6-h period (between 3 and 9 h of induction) was sufficient to generate about 40% of bacteria with a new surface antigen. This 6-h period corresponds to < 3 generations since the doubling time of this strain was 2.8 ± 0.3 h (mean ± SD, n = 3 independent experiments) under this experimental set-up.

## Discussion

The data reported here show that several components of the *B. abortus* OM are heterogeneously localized. This heterogeneity is maintained by the low mobility of individual components such as Omp2b, Omp25, and LPS over a period of time corresponding to a bacterial cell cycle (2–4 h). Additionally, the different layers of the envelope (OM and PG) are all inserted at the new pole and at the constriction site.

Initial LPS extractions of *Brucella* strains showed two distinct banding patterns in SDS-PAGE representing R-LPS and S-LPS (Dubray & Limet, 1987; Bowden *et al*, 1995; Zygmunt *et al*, 2012). Moreover, flow cytometry analysis already suggested positive signals for S-LPS and R-LPS in the smooth *B. abortus* 544 WT strain (Bowden *et al*, 1995), consistent with our estimate that a majority (~97%) of bacteria display a mix of S-LPS and R-LPS (Fig 1B). This co-existence of R-LPS and S-LPS on single bacteria would be interesting to investigate in other bacteria. Our single cell analyses using fluorescence microscopy revealed a high heterogeneity between single cells with R-LPS labeling ranging from absence to patchy and even full labeling (Figs 1A and EV1). Furthermore, in AFM analyses, the areas enriched in R-LPS correlated with a high roughness ( $R_a$ ) value (Fig 2), suggesting that irregular surface structures, already reported for *E. coli* (Amro *et al*, 2000; Gammoudi *et al*, 2016) and *S. meliloti* (Greif *et al*, 2010), correspond to mixes of long and short LPS molecules. To our knowledge, this is the first study making a correlation between the presence of R-LPS clusters localized by fluorescence microscopy and the physical surface structure of the bacterial surface investigated by AFM.

Our data also show that R-LPS clusters are co-localizing with Omp2b (Fig 3A and C, Appendix Fig S3), an essential trimeric porin predicted to be involved in nutrient uptake (Douglas *et al*, 1984). The binding of LPS molecules to different OM porins was already reported for several other Gram-negative bacteria, e.g., *E. coli* (Rocque *et al*, 1987; Strittmatter & Galanos, 1987; Buehler *et al*, 1991; de Cock & Tommassen, 1996), *Salmonella* (Strittmatter & Galanos, 1987; Latsch *et al*, 1992; Hagge *et al*, 2002) or *Yersinia* (Strittmatter & Galanos, 1987; Vakorina *et al*, 2003). This is well described for

**Figure 6. Unipolar insertion and low mobility of LPS.**

- A Localization of S-LPS (green) in the eFluor-labeled (magenta) inducible rough strain  $\Delta gmd \text{ p}_{lac}\text{-}gmd$  possessing the old pole marker PdhS-mCherry (red). The strains  $\Delta gmd$  and  $\Delta gmd \text{ p}_{lac}\text{-}gmd \text{ -IPTG}$  were used as negative controls. Scale bars: 2  $\mu\text{m}$ .
- B Quantification of S-LPS insertion from (A). Numbers are indicating mean percentages.  $n = 468$  bacteria (three biological replicates).
- C Demograph represents fluorescence profile of S-LPS labeling from (A). Cells were oriented with the old pole at the bottom of the graph by PdhS-mCherry and sorted by cell length. NFI: normalized fluorescence intensity.  $n = 468$  bacteria (three biological replicates).
- D Short pulse labeling of LPS (2 h) by Kdo-N<sub>3</sub> (green) on eFluor-labeled (magenta) bacteria expressing the old pole marker PdhS-mCherry (red). Scale bars: 2  $\mu\text{m}$ .
- E Quantification of LPS insertion sites from (D). Numbers are indicating mean percentages.  $n = 566$  bacteria (three biological replicates).
- F Demographs represent fluorescence intensities of eFluor (OM, left) and Kdo-N<sub>3</sub> (LPS, right) labeling. Cells were sorted by cell length and aligned with the old pole at the bottom of the graph by PdhS-mCherry localization. NFI: normalized fluorescence intensity.  $n = 566$  bacteria (three biological replicates).

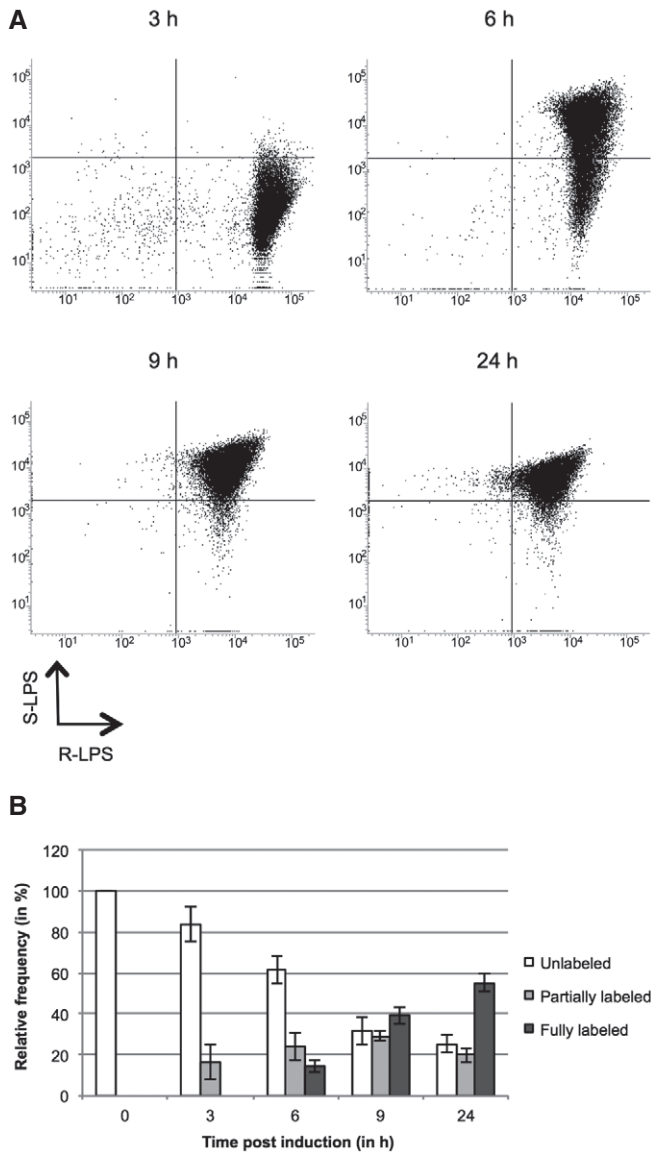


**Figure 7. Induced generation of daughter cells with S-LPS.**

- A Distribution of R-LPS and S-LPS in  $\Delta gmd$   $p_{lac}$ - $gmd$  after 3, 6, 9, and 24 h post-induction analyzed by flow cytometry (one representative example among three biological replicates,  $n = 20,000$  events).
- B Quantification of S-LPS labeling from (A) as relative frequencies. Error bars correspond to SD from 3 independent experiments.  $n_0$  h = 77 bacteria,  $n_3$  h = 254 bacteria,  $n_6$  h = 616 bacteria,  $n_9$  h = 937 bacteria,  $n_{24}$  h = 1,059 bacteria.

OmpF, a major porin of *E. coli* (Bolla *et al.*, 1988; Holzenburg *et al.*, 1989; Diedrich *et al.*, 1990; Buehler *et al.*, 1991; Sen & Nikaido, 1991; Arunmanee *et al.*, 2014, 2016; Patel *et al.*, 2016) belonging to the same family as Omp2b. One selective advantage of clustering R-LPS and Omp2b could be to facilitate diffusion of compounds from the medium into the pores of the porin, as suggested by theoretical simulations using OmpF as a model (Patel *et al.*, 2016). We were able to show that Omp2b seems to have a preference of co-localizing with R-LPS, whereas there was no distinction between the different endogenous LPS types in previous *in vivo* studies (Rocque *et al.*,

1987; Strittmatter & Galanos, 1987; Bolla *et al.*, 1988; Holzenburg *et al.*, 1989; Diedrich *et al.*, 1990; Buehler *et al.*, 1991; Latsch *et al.*, 1992). Interestingly, Omp2b clusters do not diffuse in newly inserted envelope (Fig 4D and E) suggesting that long-range diffusion of Omp2b-R-LPS clusters does not occur on *B. abortus* cell surface in the conditions tested here.

Previously, it was shown that Rhizobiales, including *B. abortus*, display unipolar growth by pulse labeling bacteria with TRSE and subsequent chase without the dye (Brown *et al.*, 2012). TRSE binds to accessible and reactive amines present on the cell surface, but up to now the insertion of a specific OM component had not been investigated. Our results indicate that the insertion of one of the major Omps of *Brucella*, namely Omp25 (Dubray & Bezard, 1980; Verstreate *et al.*, 1982; Dubray & Charriaut, 1983), is taking place mostly at the new pole in exponential phase bacteria and at the constriction site in divisional bacteria (Fig 4A and B). We found the same insertion sites for PG (Fig 5A and C), as previously reported for *A. tumefaciens* (Kuru *et al.*, 2012; Cameron *et al.*, 2014).

Localized labeling of TRSE during single cell growth assays in Rhizobiales (Brown *et al.*, 2012) is consistent with the absence of long-range diffusion of OM components. Likewise, we could show that Omp25 and Omp2b were restricted in the TRSE-positive area after a chase period (Fig 4E). This result is in agreement with the studied immobility or confinement of several Omps (see review Kleanthous *et al.*, 2015). Additionally, Omp25 and Omp2b were suggested to be bound to PG (Dubray & Bezard, 1980; Verstreate *et al.*, 1982; Dubray & Charriaut, 1983; Sowa *et al.*, 1991; Cloeckaert *et al.*, 1992b), which could explain their absence of mobility. However, the non-mobility of *E. coli* OmpA is not mediated by its ability to bind PG (Verhoeven *et al.*, 2013); thus, other mechanisms such as protein–protein interactions, as shown for BtuB-OmpF in *E. coli* (Rassam *et al.*, 2015), could contribute to the low diffusion of Omps. Detailed analysis of diffusion coefficient requiring sophisticated equipment is currently not accessible for class III pathogens but deep analysis of model bacteria like *E. coli* indicates that diffusion of OM proteins could be restricted in small patches (0.03–0.6  $\mu\text{m}$ ) (Kleanthous *et al.*, 2015; Rassam *et al.*, 2015). Confined diffusion could generate low apparent diffusion or absence of long-range diffusion as reported here for Omp25 and Omp2b.

In addition to Omp25 and PG, LPS was also inserted at the proposed growth sites (Figs 6A and D, and EV4A) and exhibited a very low apparent diffusion (Figs 6C and F, and EV4C), especially compared to LPS lateral diffusion reported for *Salmonella typhimurium* (Schindler *et al.*, 1980). However, the confinement area seems to be slightly larger for LPS compared to Omp25, since Kdo-N<sub>3</sub> labeling partially invades regions labeled with eFluor (Figs 6F and EV4C) suggesting that diffusion of LPS is less restricted than the one of Omp25 (Fig 4A). Contrary to *E. coli* LPS (Schneek *et al.*, 2010), *B. abortus* LPS does not bind massive amounts of divalent cations (Moriyon & Berman, 1982) and the lipid A comprises very long acyl chains with two of them proposed to span the OM (Velasco *et al.*, 2000). This could contribute to a deeper anchoring of LPS in the OM and therefore a reduced mobility. Moreover, the lower amount of phosphate groups present in *Brucella* LPS core could generate a lower charge repulsion between single molecules and thus a stronger interaction between them (Lapaque *et al.*, 2005). Therefore, the constraints that limit diffusion of LPS on the bacterial surface need to be further explored. Since the insertion sites of LPS are located at the

new pole and at the constriction site, it would be of great interest to localize the machinery involved, in particular LptD, a member of the LPS insertion machinery in the OM (Chng *et al*, 2010). However, as we proposed above for Omp25 and Omp2b, long-range lateral diffusion of LPS is probably very limited in the OM. The mechanisms related to the interactions between the insertion of OM proteins and LPS incorporation remain to be investigated. The combination of unipolar growth and low mobility of OM components could have an advantage in the generation of daughter cells different from their mother in terms of surface composition (Figs 7 and EV5). This would be a selective advantage in processes like phase variation and antigenic variation (van der Woude & Bäumler, 2004), which are important for bacterial pathogens. The dissociation of smooth and rough *Brucella* was already reported several years ago (Henry, 1933; Stearns & Roepke, 1941; Braun, 1945, 1946), and first suggestions were made that this dissociation could also happen inside the host (Stearns & Roepke, 1941). Genetic events leading to this dissociation have been proposed (Mancilla *et al*, 2010; Turse *et al*, 2011) and dissociation from smooth to rough was described *in vitro* as well as *in vivo* (Turse *et al*, 2011), thus highlighting the importance of this behavior regarding virulence. Our data suggest that the production of daughter cells with a different surface antigen could be achieved in a few generations (typically 2), which would contrast with a model in which surface antigens are progressively diluted along many generations to allow bacteria to escape immune surveillance (Fig EV5). This could be of particular interest for chronic pathogens with a low proliferation potential inside their hosts.

## Materials and Methods

### Bacterial strains and media

*Brucella abortus* 544 Nal<sup>R</sup> strain (referred to as WT in this study) and its derivatives were cultivated in 2YT-rich medium (1% yeast extract, 1.6% peptone, 0.5% NaCl) at 37°C. Overnight liquid cultures were diluted 10 times to a low optical density (OD<sub>600 nm</sub>), grown all day long, and diluted again in the evening to start a second overnight culture that reached an OD<sub>600 nm</sub> between 0.3 and 0.5 the next day. If not indicated otherwise, all experiments were carried out with exponential phase cultures (OD<sub>600 nm</sub> ranging from 0.3 to 0.5). *E. coli* strains were cultivated in LB medium at 37°C. All strains and plasmids used in this study are listed in Appendix Tables S1 and S2.

Antibiotics were added, if necessary, at the following concentrations: kanamycin 20 or 50 µg/ml (*kan*<sup>R</sup> at a chromosomal site or provided on a plasmid, respectively); chloramphenicol 20 µg/ml; nalidixic acid 25 µg/ml. *Brucella abortus* Δgmd p<sub>lac</sub>-gmd was induced with a final concentration of 1 mM IPTG.

### Construction of *Brucella abortus* mutant strains

Approximately 750 bp upstream and downstream of the coding sequence of interest were amplified from the purified genomic DNA of *B. abortus* 544 by PCR using Q5® High-Fidelity DNA Polymerase (New England Biolabs). These two fragments were fused by means of a 20-bp-overlapping region by PCR. The resulting amplicons were purified from agarose gels and digested as the destination vector with the corresponding restriction enzymes and ligated overnight at

20°C. Ligation products were transformed in *E. coli* DH10B, and clones were screened by PCR. Selected plasmids were checked by sequencing and transformed in *E. coli* S17-1 strain to allow conjugation to *B. abortus* 544 Nal<sup>R</sup> strain. Deletion mutants were constructed by allelic exchange via homologous recombination and checked by PCR with primers hybridizing upstream and downstream from the regions involved in recombination. The gmd coding sequence is localized in an operon containing genes involved in the synthesis of the O-chain of *B. abortus* (Godfroid *et al*, 2000). In order to avoid polar effects by the deletion of gmd, 9 bp from the end of the ORF including a ribosome-binding site remained in the genome after allelic exchange. Additionally, 15 bp downstream from the start codon was also deleted. *Brucella abortus* 544 Δgmd was complemented with the plasmid pBBR1\_gmd (p<sub>lac</sub>-gmd), which contains gmd under the control of the *E. coli* lac promoter, the *E. coli* lacI gene, and allowed a controlled induction with IPTG. The pBBR1 plasmid contains a pBBRMCS1 backbone (Kovach *et al*, 1994) and a regulation cassette originating from pSRK-Kan (Khan *et al*, 2008). It was previously validated for ctrA inducible expression in *B. abortus* (Francis *et al*, 2017). The reported plasmid contained two p<sub>lac</sub> and was thus modified as follows. In order to remove the p<sub>lac</sub> that is not used for induction, the plasmid was restricted with KpnI and SphI and the generated sticky ends were transformed to blunt-ends by T4 DNA Polymerase. The resulting plasmid was ligated, checked by sequencing, and further named pBBR1. If needed, the old pole marker PdhS-mCherry provided on pSK-Kan plasmid (*kan*<sup>R</sup>) (Van der Henst *et al*, 2010) was integrated in the genome via homologous recombination. Primers used in this study are listed in Appendix Table S3.

### TRSE and eFluor labeling

Bacteria were washed (4,600 g, 2.5 min) twice with phosphate-buffered saline (PBS) and resuspended in Texas Red™-X Succinimidyl Ester (TRSE, Invitrogen) or eBioscience™ Cell Proliferation Dye eFluor™ 670 (eFluor, Invitrogen) at a final concentration of 1 µg/ml in PBS. After 15 min of incubation at room temperature (RT) protected from light, bacteria were washed twice and resuspended either in 2YT culture medium or PBS depending on further experiment. Samples were further handled protected from light. For both labelings, a fraction of non-growing bacteria was observed at low frequency, 1.7% (4/242 bacteria) after TRSE treatment, and 3.5% (9/258 bacteria) after eFluor incubation.

### Fluorescence microscopy

Images were acquired on 1% agarose PBS pads with a Nikon Eclipse 80i fluorescence microscope equipped with a phase-contrast objective Plan Apo λ 100×/1.45 NA and a Hamamatsu camera ORCA-ER. Images were processed with NIS imaging software Elements AR (version 5.02) and further analyzed as described in the “Image analysis” section (see below). For combination of fluorescence microscopy and AFM, bacteria were imaged with an inverted fluorescence microscope Zeiss Axio Observer Z1 equipped with an EC Plan-Neofluar 100×/1.30 NA objective and a Hamamatsu camera C10600. Fluorescence images were processed with Zen imaging software 2012 (version 1.1.2.0), and AFM images were treated with JPK software (version 6.1.49).

**IF**

Different OM structures (S-LPS, R-LPS, and Omp25 and Omp2b) were localized by IF using specific mAbs (Appendix Table S4). Labeling was carried out like previously reported (Francis *et al*, 2017) with minor changes. Briefly, exponential phase bacteria were washed twice with PBS at 4,600 g for 2.5 min and resuspended in the same amount of supernatant from hybridoma culture containing the appropriate mAb. After incubation for 40 min at RT on a rotating wheel, bacteria were washed twice with PBS at 1,500 g for 2.5 min at 4°C. Pellet was resuspended in PBS containing the corresponding secondary antibody (Ab) (Appendix Table S5) diluted 1:500 and incubated for 40 min at RT on a rotating wheel. Bacteria were washed and resuspended either in 2YT medium for subsequent growth or in PBS for fluorescence microscopy. Labeling with secondary fluorescent Ab only was used as a negative control.

**Co-localization by IF**

For co-localization studies of R-LPS and S-LPS, R-LPS was initially labeled with the mAb, followed by S-LPS (Appendix Table S4) as described above. For co-localization of Omp2b and R-LPS, labeling with primary mAb was done sequentially (first Omp2b, then R-LPS), whereas both secondary fluorescent antibodies were incubated simultaneously. These secondary antibodies were isotype-specific for the primary mAb (Appendix Table S5). As a negative control, secondary antibodies with the inappropriate isotype were used to show specificity of the labeling.

**Insertion of new OM components by IF**

To monitor new insertion of Omp25 and Omp2b, bacteria were labeled with TRSE (see TRSE labeling) and afterward with a primary mAb against the structure of interest (Appendix Table S4). After washing, bacterial pellet was resuspended in prewarmed 2YT and diluted for further growth. After 2 h of growth, bacteria were labeled with secondary Ab (Appendix Table S5) and observed by fluorescence microscopy.

**Induction of S-LPS**

For the inducible strain *B. abortus* 544  $\Delta gmd$  *plac-gmd*, bacteria were labeled with eFluor (see TRSE labeling) and resuspended in prewarmed 2YT containing IPTG or not (for negative non-induced control sample). *Brucella abortus* 544  $\Delta gmd$  containing the empty vector pBBRI was used as negative control. Cultures were induced for 4 h at 37°C with shaking, washed, and then labeled by IF (see IF). Labeling was observed by fluorescence microscopy. Strains were cultivated without chloramphenicol to reduce inhibition of growth. The presence of the plasmid (pBBRI and pBBRI\_gmd) was checked after 4 h induction by plating on 2YT plates with or without chloramphenicol and counting of colony-forming units (CFU).

For the study of the induced generation of daughter cells with S-LPS, bacterial culture of  $\Delta gmd$  *plac-gmd* in early exponential phase ( $OD_{600\text{ nm}}$  around 0.1) was washed twice with PBS (4,600 g, 2.5 min) and culture was split in two parts to cultivate in induced (with IPTG) or non-induced (without IPTG) conditions.  $OD_{600\text{ nm}}$  was measured at time points 0, 3, 6, 9 and 24 h and samples were

fixed with 2% PFA. Fixed samples were labeled by IF (see above) with mAb against R-LPS and S-LPS (Appendix Tables S4 and S5) and analyzed by fluorescence microscopy and flow cytometry (see above).

**LPS labeling**

Labeling of LPS was carried out by Kdo-N<sub>3</sub> (Dumont *et al*, 2012). For short pulse labeling, exponential phase bacteria were washed twice in PBS (4,600 g, 2.5 min), labeled with eFluor, washed, and resuspended in prewarmed 2YT containing 1 mM Kdo-N<sub>3</sub>. After 2 h of growth at 37°C shaking, 50  $\mu$ l was washed twice with PBS (4,600 g, 2.5 min) and labeled for 1 h with 0.1 mM DBCO-PEG<sub>4</sub>-5/6 carboxyrhodamine 110 (Jena Bioscience) diluted in PBS protected from light on a rotating wheel (Fugier *et al*, 2015). Samples were washed and investigated by fluorescence microscopy. For long pulse labeling, bacterial culture was diluted to  $OD_{600\text{ nm}} = 0.05$  in 300  $\mu$ l 2YT 1 mM Kdo-N<sub>3</sub> and grown overnight. The cultures were washed, labeled with eFluor, and resuspended in 1.25 ml of prewarmed 2YT. After 2 h of growth, bacteria were labeled as described above and analyzed by fluorescence microscopy. As negative controls, bacteria grown in the absence of Kdo-N<sub>3</sub> were labeled with DBCO-PEG<sub>4</sub>-5/6 carboxyrhodamine 110 resulting in missing fluorescence signal.

**PG labeling**

Exponential phase bacteria were short pulse labeled for 5 min with HADA (Kuru *et al*, 2012) at a final concentration of 500  $\mu$ M in 2YT medium. Samples were treated protected from light. Cells were washed once with PBS (4,600 g, 2.5 min) and fixed with ethanol. Therefore, pellet was resuspended in 70% cold ethanol and incubated for 15 min on ice. Bacteria were washed twice with PBS and observed by fluorescence microscopy.

**AFM**

Exponential phase bacteria were washed twice with PBS (4,600 g, 2.5 min), fixed with 2% final concentration of paraformaldehyde (PFA) for 20 min at RT, and washed twice with PBS. If necessary, samples were labeled by IF as described above. For the roughness measurements, WT and  $\Delta gmd$  were labeled with the mAb directed against *Brucella* R-LPS (Appendix Table S4) and a secondary fluorescent Ab (Appendix Table S5). Bacterial concentrations were adjusted to  $10^8$  bacteria/ml and samples were stored at 4°C in PBS protected from light for maximum of 3 days. In order to prepare the sample, polyethylenimine (PEI)-coated thin glass slides were used to immobilize the cells, as described previously (Francius *et al*, 2008). Multiparametric images of bacteria were recorded in PBS using the quantitative imaging mode available on the NanoWizard III AFM (JPK Instruments, Germany).

Images were obtained using either oxide-sharpened microfabricated Si<sub>3</sub>Ni<sub>4</sub> cantilevers (MSCT; Bruker) or gold cantilevers (OMCL-TR4; Olympus, Tokyo, Japan) functionalized with mAb directed against R-LPS using protein G, as described previously (Casalini *et al*, 2015). Cells were first imaged in their entirety, at 128 pixels  $\times$  128 pixels, with an applied force kept at 0.25 nN, and a constant approach/retract speed of 20  $\mu$ m/s (z range of 500 nm). Zooms of 0.4  $\times$  0.4  $\mu$ m<sup>2</sup> were then recorded on two areas of each

bacterium. The cantilevers spring constants were determined by the thermal noise method prior to the measurements (Hutter & Bechhoefer, 1993).

The arithmetic average roughness  $R_a$  was measured on height images after order-3 flattening, and  $P_{\text{adh}}$  was determined on the adhesion images as the number of pixels with adhesion values higher than 30 pN, a threshold determined empirically to eliminate noise and unspecific interactions.

For each condition, experiments were repeated for at least 3 independent cell preparations (culture/IF).

### Image analysis

Fluorescence images were analyzed with MicrobeJ (Ducret *et al*, 2016), a plug-in of ImageJ software (Schneider *et al*, 2012). Unless otherwise stated, only isolated bacteria were analyzed and disrupted bacteria as well as cell aggregates were excluded from the analysis. For strains containing the old pole marker PdhS-mCherry, only bacteria possessing a unique polar PdhS signal were used to construct a demographic representation. For S-LPS induction in *B. abortus* 544  $\Delta gmd$   $p_{lac}$ - $gmd$ , bacteria were manually selected if necessary in smaller cell aggregates. For insertion of new Omp25, Omp2b and LPS labeling by Kdo-N<sub>3</sub>, only bacteria positive for both fluorescent labelings (TRSE/Omp25, TRSE/Omp2b, and eFluor/Kdo-N<sub>3</sub>) were analyzed. For the analysis of co-localization of Omp2b or Omp25 with TRSE, fluorescence intensities per pixel generated by MicrobeJ were used. Frequency analysis of fluorescence intensity per pixel allowed the definition of cutoffs to discriminate positive signal from background for each independent sample. These cutoffs range from 1,000 to 1,200 on a scale from 0 to 4,000 (saturation) of fluorescence intensity for Omp25 labeling, 600 for Texas Red and 800 for Omp2b labeling. The proportions of Omp2b (three samples with 17,236, 19,262, and 38,132 pixels)- or Omp25 (five samples with 10,292, 15,358, 17,672, 19,073 and 23,271 pixels)-positive signals in TRSE-positive and TRSE-negative areas were compared using a *t*-test. The co-localization analysis of Omp2b with R-LPS signals was also performed by the discrimination between positive and negative signals based on fluorescence intensity per pixel (100,382 pixels were considered), and then a chi-square test was applied with the null hypothesis that co-localization was a product of the proportion of positive signal for each labeling. Several cutoffs were considered and all yielded *P*-values  $< 10^{-40}$ .

### Flow cytometry

Late exponential phase bacteria ( $\text{OD}_{600 \text{ nm}} \approx 0.6$ ) were washed twice with PBS, fixed with 2% PFA for 20 min at RT, washed again, and labeled with mAb directed against S-LPS and R-LPS by IF (see above). Secondary antibodies (Appendix Table S5) were isotype-specific for primary antibodies. Analysis was carried with FACS-Verve™ (BD). 20,000 events were recorded per sample. The further analyzed population was defined by measuring SSC and FSC values, which allowed exclusion of small particles as well as taller aggregates. Fluorescence intensities corresponding to secondary Ab binding were recorded and presented in dot plots. The gate for each individual experiment was chosen according to the negative control, where bacteria were only labeled with secondary fluorescent antibodies.

### Statistics

Pixel analysis of co-localization of Omp2b with R-LPS generated comparisons of frequencies that were tested with a chi-square test based on the null hypothesis of independent localization probability. Comparisons of two samples were performed with one-tailed statistical tests, either *t*-test for a symmetric distribution, or Mann–Whitney *U*-test if distribution is asymmetric. With more than two samples, pairwise comparison of samples was made with Tukey test. Sample sizes and *P*-values are indicated in figure legends or in the main text.

**Expanded View** for this article is available online.

### Acknowledgements

We thank Ignacio Moriyón, Raquel Conde Álvarez, Francesco Renzi, Jean-Yves Matroule, and Jean-François Collet for stimulating and helpful discussion. We thank Stéphane Vincent and his team for the synthesis of HADA and Boris Vauzeilles for providing Kdo-N<sub>3</sub>. We thank Kévin Willemart for the technical assistance in flow cytometry and Beatriz Izquierdo Lafuente for providing the *B. abortus*  $\Delta$ omp25 strain. This research has been funded by grants from Fonds de la Recherche Scientifique–Fonds National de la Recherche Scientifique (FRS-FNRS, <http://www.fnrs.be>) (PDR T.0053.13 and PDR Brucell-cycle T.0060.15, and CDR J.0091.14) to X. De Bolle. The work was also funded by a grant from Concerted Research Actions (17/22-087) of the Fédération Wallonie-Bruxelles, to J.-F. Collet, P. Soumillion and X. De Bolle. We thank UNamur (<https://www.unamur.be/>) for financial and logistic support. V. Vassen is supported by a Ph.D. grant from FRIA (FRS-FNRS). Work at the Université Catholique de Louvain was supported by the European Research Council (ERC) under the European Union's Horizon 2020 research and innovation program (grant agreement 693630), the FRS-FNRS, the FNRS-WELBIO (grant WELBIO-CR-2015A-05), and the Research Department of the Communauté Française de Belgique (Concerted Research Action). Y.F. Dufrêne is a Research Director at FNRS.

### Author contributions

VV performed all experiments except AFM experiments, which were performed by CV, CF, and CF-D; VV and XDB designed the study and CV, CF, CF-D, and YFD designed the AFM experiments; VV and XDB wrote the manuscript; CV and CF wrote the manuscript concerning AFM experiments; all authors read and approved the final manuscript.

### Conflict of interest

The authors declare that they have no conflict of interest.

### References

- Amro NA, Kotra LP, Wadu-Mesthrige K, Bulychev A, Mabashery S, G-y L (2000) High-resolution atomic force microscopy studies of the *Escherichia coli* outer membrane: structural basis for permeability. *Langmuir* 16: 2789–2796
- Arunmanee W, Harris JR, Lakey JH (2014) Outer membrane protein F stabilised with minimal amphipol forms linear arrays and LPS-dependent 2D crystals. *J Membr Biol* 247: 949–956
- Arunmanee W, Pathania M, Solovyova AS, Le Brun AP, Ridley H, Basle A, van den Berg B, Lakey JH (2016) Gram-negative trimeric porins have specific LPS binding sites that are essential for porin biogenesis. *Proc Natl Acad Sci USA* 113: E5034–E5043
- Beveridge TJ (1999) Structures of gram-negative cell walls and their derived membrane vesicles. *J Bacteriol* 181: 4725–4733

- Bolla JM, Lazdunski C, Pages JM (1988) The assembly of the major outer membrane protein OmpF of *Escherichia coli* depends on lipid synthesis. *EMBO J* 7: 3595–3599
- Bowden RA, Cloeckaert A, Zygmunt MS, Bernard S, Dubray G (1995) Surface exposure of outer membrane protein and lipopolysaccharide epitopes in *Brucella* species studied by enzyme-linked immunosorbent assay and flow cytometry. *Infect Immun* 63: 3945–3952
- Braun W (1945) Factors controlling bacterial dissociation. *Science* 101: 182–183
- Braun W (1946) Dissociation in *Brucella abortus*: a demonstration of the role of inherent and environmental factors in bacterial variation. *J Bacteriol* 51: 327–349
- Brown PJ, de Pedro MA, Kysela DT, Van der Henst C, Kim J, De Bolle X, Fuqua C, Brun YV (2012) Polar growth in the alphaproteobacterial order rhizobiales. *Proc Natl Acad Sci USA* 109: 1697–1701
- Buehler LK, Kusumoto S, Zhang H, Rosenbusch JP (1991) Plasticity of *Escherichia coli* porin channels. Dependence of their conductance on strain and lipid environment. *J Biol Chem* 266: 24446–24450
- Burman LG, Raichler J, Park JT (1983) Evidence for diffuse growth of the cylindrical portion of the *Escherichia coli* murein sacculus. *J Bacteriol* 155: 983–988
- Cameron TA, Anderson-Furgeson J, Zupan JR, Zik JJ, Zambryski PC (2014) Peptidoglycan synthesis machinery in *Agrobacterium tumefaciens* during unipolar growth and cell division. *MBio* 5: e01219-14
- Cardoso PG, Macedo GC, Azevedo V, Oliveira SC (2006) *Brucella* spp noncanonical LPS: structure, biosynthesis, and interaction with host immune system. *Microb Cell Fact* 5: 13
- Casalini S, Dumitru AC, Leonardi F, Bortolotti CA, Herruzo ET, Campana A, de Oliveira RF, Cramer T, Garcia R, Biscarini F (2015) Multiscale sensing of antibody-antigen interactions by organic transistors and single-molecule force spectroscopy. *ACS Nano* 9: 5051–5062
- Chng SS, Ruiz N, Chimalakonda G, Silhavy TJ, Kahne D (2010) Characterization of the two-protein complex in *Escherichia coli* responsible for lipopolysaccharide assembly at the outer membrane. *Proc Natl Acad Sci USA* 107: 5363–5368
- Chopinet L, Formosa C, Rols MP, Duval RE, Dague E (2013) Imaging living cells surface and quantifying its properties at high resolution using AFM in QI mode. *Micron* 48: 26–33
- Cloeckaert A, de Wergifosse P, Dubray G, Limet JN (1990) Identification of seven surface-exposed *Brucella* outer membrane proteins by use of monoclonal antibodies: immunogold labeling for electron microscopy and enzyme-linked immunosorbent assay. *Infect Immun* 58: 3980–3987
- Cloeckaert A, Jacques I, de Wergifosse P, Dubray G, Limet JN (1992a) Protection against *Brucella melitensis* or *Brucella abortus* in mice with immunoglobulin G (IgG), IgA, and IgM monoclonal antibodies specific for a common epitope shared by the *Brucella* A and M smooth lipopolysaccharides. *Infect Immun* 60: 312–315
- Cloeckaert A, Zygmunt MS, de Wergifosse P, Dubray G, Limet JN (1992b) Demonstration of peptidoglycan-associated *Brucella* outer-membrane proteins by use of monoclonal antibodies. *J Gen Microbiol* 138: 1543–1550
- Cloeckaert A, Jacques I, Bowden RA, Dubray G, Limet JN (1993) Monoclonal antibodies to *Brucella* rough lipopolysaccharide: characterization and evaluation of their protective effect against *B. abortus*. *Res Microbiol* 144: 475–484
- de Cock H, Tommassen J (1996) Lipopolysaccharides and divalent cations are involved in the formation of an assembly-competent intermediate of outer-membrane protein PhoE of *E. coli*. *EMBO J* 15: 5567–5573
- Conde-Alvarez R, Arce-Gorvel V, Iriarte M, Mancek-Keber M, Barquero-Calvo E, Palacios-Chaves L, Chacon-Diaz C, Chaves-Olarte E, Martirosyan A, von Bargen K, Grillo MJ, Jerala R, Brandenburg K, Llobet E, Bengoechea JA, Moreno E, Moriyon I, Gorvel JP (2012) The lipopolysaccharide core of *Brucella abortus* acts as a shield against innate immunity recognition. *PLoS Pathog* 8: e1002675
- Diedrich DL, Stein MA, Schnaitman CA (1990) Associations of *Escherichia coli* K-12 OmpF trimers with rough and smooth lipopolysaccharides. *J Bacteriol* 172: 5307–5311
- Douglas JT, Rosenberg EY, Nikaido H, Verstreate DR, Winter AJ (1984) Porins of *Brucella* species. *Infect Immun* 44: 16–21
- Dubray G, Bezard G (1980) Isolation of three *Brucella abortus* cell-wall antigens protective in murine experimental brucellosis. *Ann Rech Vet* 11: 367–373
- Dubray G, Charraut C (1983) Evidence of three major polypeptide species and two major polysaccharide species in the *Brucella* outer membrane. *Ann Rech Vet* 14: 311–318
- Dubray G, Limet J (1987) Evidence of heterogeneity of lipopolysaccharides among *Brucella* biovars in relation to A and M specificities. *Ann Inst Pasteur Microbiol* 138: 27–37
- Ducret A, Quardokus EM, Brun YV (2016) MicrobeJ, a tool for high throughput bacterial cell detection and quantitative analysis. *Nat Microbiol* 1: 16077
- Dumont A, Malleron A, Awwad M, Dukan S, Vauzeilles B (2012) Click-mediated labeling of bacterial membranes through metabolic modification of the lipopolysaccharide inner core. *Angew Chem Int Ed Engl* 51: 3143–3146
- Formosa C, Grare M, Jauvert E, Coutable A, Regnouf-de-Vains JB, Mourer M, Duval RE, Dague E (2012) Nanoscale analysis of the effects of antibiotics and CX1 on a *Pseudomonas aeruginosa* multidrug-resistant strain. *Sci Rep* 2: 575
- Francis N, Poncin K, Fioravanti A, Vassen V, Willemart K, Ong TA, Rappez L, Letesson JJ, Biondi EG, De Bolle X (2017) CtrA controls cell division and outer membrane composition of the pathogen *Brucella abortus*. *Mol Microbiol* 103: 780–797
- Francius G, Tesson B, Dague E, Martin-Jezequel V, Dufrene YF (2008) Nanostructure and nanomechanics of live *Phaeodactylum tricornutum* morphotypes. *Environ Microbiol* 10: 1344–1356
- Fugier E, Dumont A, Malleron A, Poquet E, Mas Pons J, Baron A, Vauzeilles B, Dukan S (2015) Rapid and specific enrichment of culturable gram negative bacteria using non-lethal copper-free click chemistry coupled with magnetic beads separation. *PLoS ONE* 10: e0127700
- Gammoudi I, Mathelie-Guinlet M, Morote F, Beven L, Moynet D, Grauby-Heywang C, Cohen-Bouhacina T (2016) Morphological and nanostructural surface changes in *Escherichia coli* over time, monitored by atomic force microscopy. *Colloids Surf B Biointerfaces* 141: 355–364
- Gil-Ramirez Y, Conde-Alvarez R, Palacios-Chaves L, Zuniga-Ripa A, Grillo MJ, Arce-Gorvel V, Hanniffy S, Moriyon I, Iriarte M (2014) The identification of *wadB*, a new glycosyltransferase gene, confirms the branched structure and the role in virulence of the lipopolysaccharide core of *Brucella abortus*. *Microb Pathog* 73: 53–59
- Godfroid F, Cloeckaert A, Taminiua B, Danese I, Tibor A, De Bolle X, Mertens P, Letesson JJ (2000) Genetic organisation of the lipopolysaccharide O-antigen biosynthesis region of *Brucella melitensis* 16M (wbk). *Res Microbiol* 151: 655–668
- Greif D, Wesner D, Regtmeier J, Anselmetti D (2010) High resolution imaging of surface patterns of single bacterial cells. *Ultramicroscopy* 110: 1290–1296
- Hagge SO, de Cock H, Gutsmann T, Beckers F, Seydel U, Wiese A (2002) Pore formation and function of phosphoprotein PhoE of *Escherichia coli* are determined by the core sugar moiety of lipopolysaccharide. *J Biol Chem* 277: 34247–34253

- Hallez R, Mignolet J, Van Mullem V, Wery M, Vandenhoute J, Letesson JJ, Jacobs-Wagner C, De Bolle X (2007) The asymmetric distribution of the essential histidine kinase PdhS indicates a differentiation event in *Brucella abortus*. *EMBO J* 26: 1444–1455
- Henry BS (1933) Dissociation in the genus *Brucella*. *J Infect Dis* 52: 374–402
- Holzenburg A, Engel A, Kessler R, Manz HJ, Lustig A, Aebi U (1989) Rapid isolation of OmpF porin-LPS complexes suitable for structure-function studies. *Biochemistry* 28: 4187–4193
- Hutter JL, Bechhoefer J (1993) Calibration of atomic-force microscope tips. *Rev Sci Instrum* 64: 1868–1873
- Khan SR, Gaines J, Roop RM II, Farrand SK (2008) Broad-host-range expression vectors with tightly regulated promoters and their use to examine the influence of TraR and TraM expression on Ti plasmid quorum sensing. *Appl Environ Microbiol* 74: 5053–5062
- Kleanthous C, Rassam P, Baumann CG (2015) Protein-protein interactions and the spatiotemporal dynamics of bacterial outer membrane proteins. *Curr Opin Struct Biol* 35: 109–115
- Kovach ME, Phillips RW, Elzer PH, Roop RM II, Peterson KM (1994) pBBR1MCS: a broad-host-range cloning vector. *Biotechniques* 16: 800–802
- Kuru E, Hughes HV, Brown PJ, Hall E, Tekkam S, Cava F, de Pedro MA, Brun YV, VanNieuwenhze MS (2012) *In situ* probing of newly synthesized peptidoglycan in live bacteria with fluorescent D-amino acids. *Angew Chem Int Ed Engl* 51: 12519–12523
- Lapaque N, Moriyon I, Moreno E, Gorvel JP (2005) *Brucella* lipopolysaccharide acts as a virulence factor. *Curr Opin Microbiol* 8: 60–66
- Latsch M, Stemmer F, Loos M (1992) Purification and characterization of LPS-free porins isolated from *Salmonella minnesota*. *FEMS Microbiol Lett* 69: 275–281
- Mancilla M, Lopez-Goni I, Moriyon I, Zarraga AM (2010) Genomic island 2 is an unstable genetic element contributing to *Brucella* lipopolysaccharide spontaneous smooth-to-rough dissociation. *J Bacteriol* 192: 6346–6351
- Mobasher H, Ficht TA, Marquis H, Lea EJ, Lakey JH (1997) *Brucella* Omp2a and Omp2b porins: single channel measurements and topology prediction. *FEMS Microbiol Lett* 155: 23–30
- Moreno E, Moriyón I (2006) The genus *Brucella*. In *The prokaryotes: volume 5: proteobacteria: alpha and beta subclasses*, Dworkin M, Falkow S, Rosenberg E, Schleifer K-H, Stackebrandt E (eds), pp 315–456. New York, NY: Springer New York
- Moriyon I, Berman DT (1982) Effects of nonionic, ionic, and dipolar ionic detergents and EDTA on the *Brucella* cell envelope. *J Bacteriol* 152: 822–828
- Nikaido H, Vaara M (1985) Molecular basis of bacterial outer membrane permeability. *Microbiol Rev* 49: 1–32
- Paquet JY, Diaz MA, Genevois S, Grayon M, Verger JM, de Bolle X, Lakey JH, Letesson JJ, Cloeckaert A (2001) Molecular, antigenic, and functional analyses of Omp2b porin size variants of *Brucella* spp. *J Bacteriol* 183: 4839–4847
- Patel DS, Re S, Wu EL, Qi Y, Klebba PE, Widmalm G, Yeom MS, Sugita Y, Im W (2016) Dynamics and interactions of OmpF and LPS: influence on pore accessibility and ion permeability. *Biophys J* 110: 930–938
- de Pedro MA, Quintela JC, Holtje JV, Schwarz H (1997) Murein segregation in *Escherichia coli*. *J Bacteriol* 179: 2823–2834
- Rassam P, Copeland NA, Birkholz O, Toth C, Chavent M, Duncan AL, Cross SJ, Housden NG, Kaminska R, Seger U, Quinn DM, Garrod TJ, Sansom MS, Piehler J, Baumann CG, Kleanthous C (2015) Supramolecular assemblies underpin turnover of outer membrane proteins in bacteria. *Nature* 523: 333–336
- Rocque WJ, Coughlin RT, McGroarty EJ (1987) Lipopolysaccharide tightly bound to porin monomers and trimers from *Escherichia coli* K-12. *J Bacteriol* 169: 4003–4010
- Schindler M, Osborn MJ, Koppel DE (1980) Lateral diffusion of lipopolysaccharide in the outer membrane of *Salmonella typhimurium*. *Nature* 285: 261–263
- Schneck E, Schubert T, Konovalov OV, Quinn BE, Gutmann T, Brandenburg K, Oliveira RG, Pink DA, Tanaka M (2010) Quantitative determination of ion distributions in bacterial lipopolysaccharide membranes by grazing-incidence X-ray fluorescence. *Proc Natl Acad Sci USA* 107: 9147–9151
- Schneider CA, Rasband WS, Eliceiri KW (2012) NIH image to ImageJ: 25 years of image analysis. *Nat Methods* 9: 671–675
- Sen K, Nikaido H (1991) Lipopolysaccharide structure required for *in vitro* trimerization of *Escherichia coli* OmpF porin. *J Bacteriol* 173: 926–928
- Sowa BA, Kelly KA, Ficht TA, Frey M, Adams LG (1991) SDS-soluble and peptidoglycan-bound proteins in the outer membrane-peptidoglycan complex of *Brucella abortus*. *Vet Microbiol* 27: 351–369
- Stearns TW, Roepke MH (1941) The effect of dissociation on the electrophoretic mobility of *Brucella*. *J Bacteriol* 42: 745–755
- Strittmatter W, Galanos C (1987) Characterisation of protein co-extracted together with LPS in *Escherichia coli*, *Salmonella minnesota* and *Yersinia enterocolitica*. *Microp Pathog* 2: 29–36
- Turse JE, Pei J, Ficht TA (2011) Lipopolysaccharide-deficient *Brucella* variants arise spontaneously during infection. *Front Microbiol* 2: 54
- Vakorina TI, Novikova OD, Krasikova IN, Naberezhnykh GN, Solov'eva TF, Ovodov YS (2003) Interaction of porin from *Yersinia pseudotuberculosis* with different structural forms of endogenous lipopolysaccharide. *Biochemistry* 68: 976–983
- Van der Henst C, Charlier C, Deghele M, Wouters J, Matroule JY, Letesson JJ, De Bolle X (2010) Overproduced *Brucella abortus* PdhS-mCherry forms soluble aggregates in *Escherichia coli*, partially associating with mobile foci of Ibpa-YFP. *BMC Microbiol* 10: 248
- Velasco J, Bengoechea JA, Brandenburg K, Lindner B, Seydel U, Gonzalez D, Zahringer U, Moreno E, Moriyon I (2000) *Brucella abortus* and its closest phylogenetic relative, *Ochrobactrum* spp., differ in outer membrane permeability and cationic peptide resistance. *Infect Immun* 68: 3210–3218
- Verhoeven GS, Dogterom M, den Blaauwen T (2013) Absence of long-range diffusion of OmpA in *E. coli* is not caused by its peptidoglycan binding domain. *BMC Microbiol* 13: 66.
- Verstreate DR, Creasy MT, Caveney NT, Baldwin CL, Blab MW, Winter AJ (1982) Outer membrane proteins of *Brucella abortus*: isolation and characterization. *Infect Immun* 35: 979–989
- Wientjes FB, Nanninga N (1989) Rate and topography of peptidoglycan synthesis during cell division in *Escherichia coli*: concept of a leading edge. *J Bacteriol* 171: 3412–3419
- Woldringh CL, Huls P, Pas E, Brakenhoff GJ, Nanninga N (1987) Topography of peptidoglycan synthesis during elongation and polar cap formation in a cell division mutant of *Escherichia coli* MC4100. *Microbiology* 133: 575–586
- van der Woude MW, Bäumler AJ (2004) Phase and antigenic variation in bacteria. *Clin Microbiol Rev* 17: 581–611
- Zygmunt MS, Jacques I, Bernardet N, Cloeckaert A (2012) Lipopolysaccharide heterogeneity in the atypical group of novel emerging *Brucella* species. *Clin Vaccine Immunol* 19: 1370–1373